Journal Pre-proofs

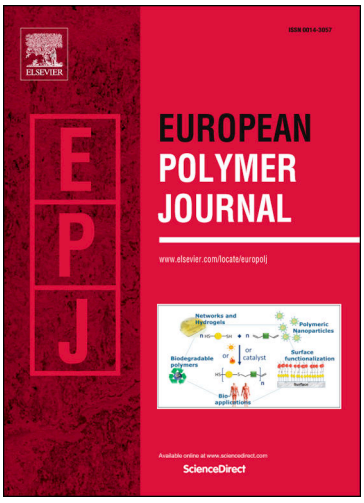

Carbazole-Pyridazine copolymers and their rhenium complexes: effect of the molecular structure on the electronic properties

Stefania Zappia, Lorenzo Veronese, Alessandra Forni, Sandro Dattilo, Filippo Samperi, Janardan Dagar, Thomas M. Brown, Monica Panigati, Silvia Destri

PII: S0014-3057(22)00099-4
DOI: https://doi.org/10.1016/j.eurpolymj.2022.111095
Reference: EPJ 111095

To appear in: *European Polymer Journal*

Received Date: 2 September 2021
Revised Date: 4 February 2022
Accepted Date: 23 February 2022

Please cite this article as: Zappia, S., Veronese, L., Forni, A., Dattilo, S., Samperi, F., Dagar, J., Brown, T.M., Panigati, M., Destri, S., Carbazole-Pyridazine copolymers and their rhenium complexes: effect of the molecular structure on the electronic properties, *European Polymer Journal* (2022), doi: https://doi.org/10.1016/j.eurpolymj.2022.111095

Carbazole-Pyridazine copolymers and their rhenium complexes: effect of the molecular structure on the electronic properties

Stefania Zappia[a,*], Lorenzo Veronese[b], Alessandra Forni[c], Sandro Dattilo[d], Filippo Samperi[d,*], Janardan Dagar[e,f], Thomas M. Brown[e], Monica Panigati[b,g], Silvia Destri[a,*]

[a] *Istituto di Scienze e Tecnologie Chimiche "Giulio Natta" (SCITEC), CNR, via Alfonso Corti 12, 20133, Milano, Italy*
[b] *Dipartimento di Chimica, Università degli Studi di Milano, via Camillo Golgi 19, 20133, Milano, Italy*
[c] *Istituto di Scienze e Tecnologie Chimiche "Giulio Natta" (SCITEC), CNR, via Camillo Golgi 19, 20133, Milano, Italy*
[d] *Istituto dei Polimeri, Compositi e Biomateriali (IPCB), CNR, via Paolo Gaifami 18, 95126, Catania, Italy*
[e] *Centre for Hybrid and Organic Solar Energy, Department of Electronic Engineering, University of Rome Tor Vergata, via del Politecnico 1,00133, Rome, Italy*
[f] *Present address: Helmholtz-Zentrum Berlin für Materialien und Energie, Young Investigator Group Hybrid Materials Formation and Scaling, Kekuléstraße 5, D-12489 Berlin, Germany*
[g] *Consorzio INSTM, via G. Giusti 9, 50121, Firenze, Italy*

Abstract

Two new push-pull copolymers, poly[*N*-(9-heptadecanyl)carbazole-2,7-diyl-*alt*-phthalazine- 5,8-diyl] (**P1**) and poly[*N*-(9-heptadecanyl)carbazole-2,7-diyl-*alt*-thieno[3,4-*d*]pyridazine- 5,7-diyl] (**P2)**, were synthetized by means of a Suzuki polycondensation. The molecular characterization with ^{1}H-NMR and MALDI-MS showed enchainment defects in the polymer backbones depending on the synthetic conditions (catalyst and temperature). Both carbazole-carbazole and diazine-diazine homocoupling defects occurred, particularly in the case of P2. For P1, instead, almost homocoupling-free material was obtained. Exploiting the metal coordination capability of the pyridazine ring, corresponding dinuclear rhenium-based metallopolymers, **ReP1** and **ReP2**, were also synthetized. All materials were investigated with experimental techniques (UV-vis spectroscopy, photoluminescence, cyclic voltammetry) and corroborated by theoretical studies (DFT and TD-DFT), including a qualitative evaluation of the effects of backbone defects on the electronic properties of the polymers. They were also tested in organic photovoltaic (OPV) devices. The wide energy gaps (E_g) accompanied with a low absorption coefficient for the band in the visible range reduced the harvesting capability of the copolymers. These drawbacks were partially overcome in the metallopolymers. The low device performance was mainly attributable to the low solubility of the metallopolymers in the organic solvents.

Keywords: Suzuki coupling, homocoupling, semiconducting polymers, pyridazine, rhenium, OPV

1. Introduction

Many factors must be taken in consideration for the development of highly efficient organic photovoltaic (OPV) devices. For obtaining effective donor and acceptor materials, the primary concerns include design and preparation of materials with appropriate energy gaps (E_g) and energy levels in order to maximize both the short circuit current (J_{SC}) and the open circuit voltage (V_{OC}), foster good charge carrier mobilities through the planarization of polymers, along with good π–π stacking characteristics, and develop stable materials, all while maintaining their solution processability.

Chemical design strategies to improve optical and electrical properties include the introduction of fused heterocyclic rings to increase the electron mobility in the π-conjugated system, or the addition of electron withdrawing moieties or again the alternation of electron poor and electron rich units along the backbone to narrow the E_g.[1-3] In the last scenario the semiconducting polymers are constituted by a so-called "push-pull" system, and their properties depend on the ability of both moieties to provide and to withdraw electrons, respectively.

Among heteroaryl moieties, nitrogen-containing heterocycles were used either as single rings or in fused systems, alternated with thiophene units[4, 5] or with other electron-rich heteroaromatic rings, such as carbazole,[6]. They were also used as electron rich moieties alternated with benzothiadiazole[7] in order to obtain low-band-gap (LBG) polymers.

In this framework, pyridazine containing bis-imine aromatic nitrogen atoms represent promising candidates to be incorporated as the electron-withdrawing portion in organic conjugated molecules and polymers, because of their electron-deficient character, favoring intramolecular charge transfer (ICT). Monomeric 1,4- and 1,3-diazines[8] (**Fig. 1**, **1** and **2** respectively) and their derivatives, in particular quinoxaline (**4**)[9-11] and thieno[3,4-*b*]pyrazine (**5**),[12, 13] were used in the design of LBG and medium band gap oligomers and polymers. Otherwise, to the best of our knowledge, the 1,2-diazines, pyridazine (**3**) and particularly its benzo- and thieno-derivatives, namely phthalazine and thieno[3,4-*d*]pyridazine (**Fig. 1**, **8** and **9** respectively) were not systematically investigated and generally in the literature the electron donating moiety of the "push-pull" system is directly connected to the diazine ring.[5, 14-16] The literature reports few examples with the diazine ring in a side position with respect to the main backbone,[17] that makes the system ambipolar, particularly if the electron withdrawing moiety is constituted by a thiophene-diazine-thiophene system.[7] Furthermore, pyridazine is the most basic among the three different diazines with a pK_a value of 2.33,[18] and it can act as bridging ligand in transition metal complexes through the nitrogen lone pair.[19]

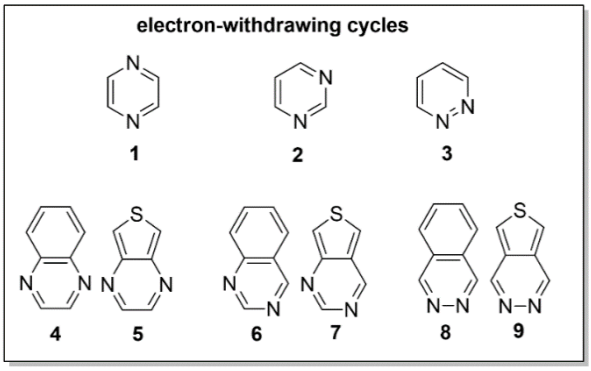

Fig. 1 Diazine-based six-member heterocycles and electron withdrawing power scale: 1,2-diazine (3) < 1,3-diazine (2) <1,4-diazine (1).

Another possible strategy to tune E_g increasing the material light harvesting ability and even enlarging its absorption in the near-infrared spectrum consists in the introduction of either a transition metal, or its complex, in the polymeric backbone,[20, 21] providing a hybrid material with new properties.[22] Different strategies for anchoring a metal-containing fragment directly in the main chain or on the side of a conducting polymer were reported. The final properties of the metallopolymers were addressed. In particular the coordination of the metal fragment extends the absorption coverage, and improves the hole mobility and the charge transfer properties of the polymers.[23-26]

A huge number of studies on metal-containing conductive polymers for optoelectronic applications involves heterocyclic nitrogen ligands capable of anchoring metals such as iridium,[27] ruthenium or platinum,[20, 28] while less attention was paid to metallopolymers containing rhenium.[28-31] Moreover, only in few cases these rhenium-based metallopolymers were studied as component for bulk heterojunction solar cells.[20, 32-34]

Recently, a novel class of dinuclear Re(I) complexes based on bridging diazines, which exhibit photoluminescence efficiencies that are much higher than those of traditional mononuclear Re(I) complexes, was reported.[35, 36] The possibility of tuning the band gap by modifying the ancillary ligands[37, 38] or the diazine substituents, was already demonstrated and exploited to red-shift the wavelength of absorption.[39, 40]

In this paper we report the synthesis of new push-pull widegap copolymers obtained by combining carbazole unit with two electron-poor units, namely phthalazine and thieno[3,4-*d*]pyridazine (**Fig. 1**, **8** and **9** respectively). Exploiting the metal coordination of the nitrogen atom in the aromatic ring, the corresponding metallopolymer, containing Re(I) complexes, were also synthetized.

The effect of the withdrawing characteristics of these two diazines was compared with that of benzothiadiazole showing a higher electron accepting ability,[41] used as monomeric unit in a push-pull copolymer with carbazole.[42-44] Characterizations of the materials from a molecular point of view, namely ^{1}H-nuclear magnetic resonance (^{1}H-NMR), size exclusion chromatography (SEC), and matrix-assisted laser desorption/ionization-time of flight mass spectrometry (MALDI-TOF MS) to determine backbone enchainment were performed, together with cyclic voltammetric (CV) analysis and optical characterization (UV-vis spectroscopy, photoluminescence), in solution. Time-Dependent Density-Functional Theory (TD-DFT) calculations were carried out to interpret and correlate electrochemical and spectroscopic data. OPV devices with each copolymer and with their related metallopolymers were prepared and their performances reported.

2. Results and discussion

Synthesis and molecular characterization. Two electron poor monomers, namely 5,8-dibromophtalazine and 5,7-dibromothieno[3,4-*d*]pyridazine (**Scheme 1**, **10-M1** and **11-M2** respectively), were chosen as co-monomers in the polymerization reaction. They were synthesized starting from the brominated precursor of either dibenzyliden-hydrazine or 1,2-bis(thiophen-3-ylmethylene)hydrazine, respectively (see supplementary material).[45] Two new alternating push-pull copolymers poly[*N*-(9-heptadecanyl)carbazole-2,7-diyl-*alt*-phthalazine-5,8-diyl] and poly[*N*-(9-heptadecanyl)carbazole-2,7-diyl-*alt*-thieno[3,4-*d*]pyridazine-5,7-diyl, hereafter **P1** and **P2** respectively, were obtained exploiting a typical Suzuki polycondensation (SPC) starting from 9-(heptadecan-9-yl)-2,7-bis(4,4,5,5-tetramethyl-1,3,2-dioxaborolan-2-yl)-9*H*-carbazole (**Scheme 1**,

12) and the two properly dibrominated co-monomers **10-M1** and **11-M2** respectively, as sketched in **Scheme 1**. The overall polymerization conditions are reported in **Table 1**.

A typical SPC was performed in toluene at high temperature for 70 hours, with the final addition of 5-methylthiophene-2-boronic acid pinacol ester for quenching the growth of the polymeric chains. The branched long alkyl chain as N-substituent on carbazole unit was chosen to ensure good solubility in organic solvents and to increase the film forming capability of the resulting copolymers. In fact, **P1** and **P2** were found to be soluble in common organic solvents (toluene, chloroform, dichloromethane, and other chlorinated solvents).

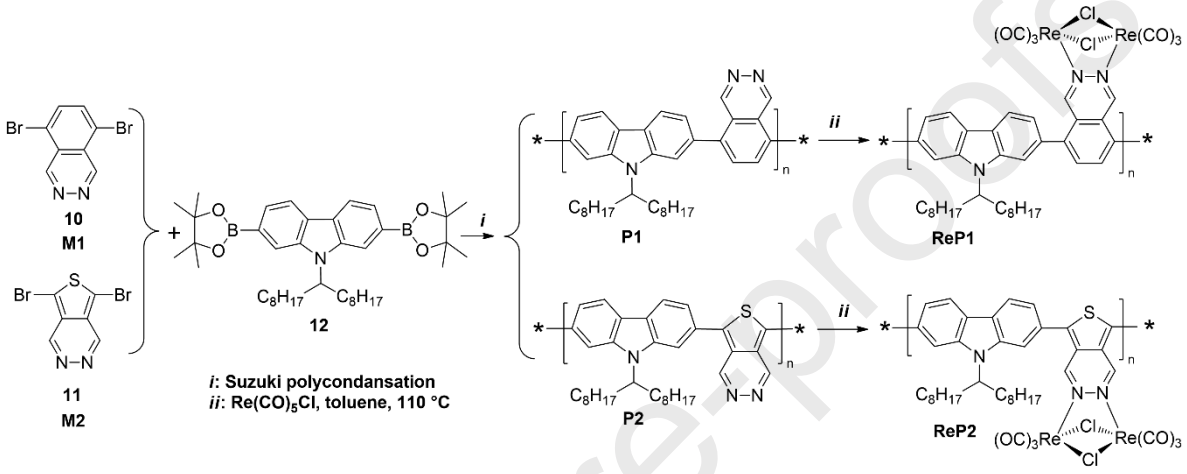

Scheme 1 Synthetic routes for the synthesis of P1 and P2, and the corresponding metallopolymers ReP1 and ReP2.

The catalysts for the SPC were selected according to their stability in air and activity, as reported in the literature.[46] In particular, in the case of **P1**, tris(benzylideneacetone)dipalladium(0) with tri(*o*-tolyl)phosphine ($Pd_2(dba)_3$)/P(*o*-tol)$_3$) was used as the catalytic system, leading to products with appreciable molar masses (MM) and good yield (**Fig 2a** and **Table 1**). Unfortunately, the same procedure was ineffective to achieve **P2**, providing only short oligomers (dimers and trimers from MALDI-MS, M_n = 1220 Da) starting from **M2** with rather low diazine insertion in the backbone, as shown in the ^{1}H-NMR spectrum (**Fig 2b** and **Table 1**).

Table 1 Reaction conditions and yield of Suzuki polymerization of 9-(heptadecan-9-yl)-2,7-bis(4,4,5,5-tetramethyl-1,3,2-dioxaborolan-2-yl)-9H-carbazole (12) with 5,8-dibromophtalazine (**M1**) and 5,7-dibromothieno[3,4-d]pyridazine (**M2**) for the synthesis of **P1** and **P2**.

sample	catalytic system	K_2CO_3 [eq]	T [°C]	yield [%]
P1-run1	$Pd_2(dba)_3$ 1%/P(*o*-tol)$_3$ 4%	2	90	12
P1-run2	$Pd_2(dba)_3$ 1%/P(*o*-tol)$_3$ 4%	10	90	51
P1-run3	$Pd_2(dba)_3$ 1%/P(*o*-tol)$_3$ 4%	10	100	69
P1-run4	$Pd_2(dba)_3$ 1%/P(*o*-tol)$_3$ 4%	10	110	75

P2-run1	$Pd_2(dba)_3$ 1%/P(*o*-tol)$_3$ 4%	10	90	39
P2-run2	$Pd(PPh_3)_4$ 1%	4	90	24
P2-run3	$Pd(PPh_3)_4$ 1%	4	100	50
P2-run4	$Pd(PPh_3)_4$ 1%	4	110	68

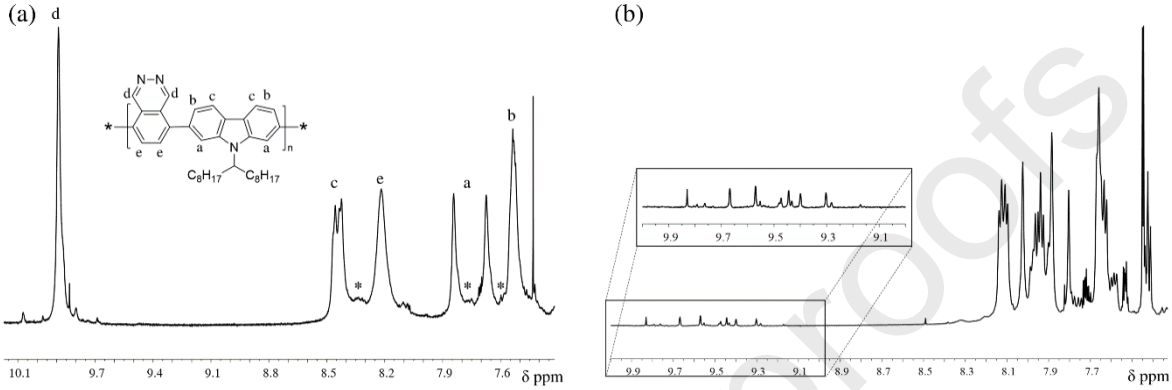

Fig. 2 ^{1}H NMR spectra of (a) **P1**, and (b) **P2-run1** performed in CDCl3, 300K, 400 MHz (expansion in the aromatic region between 10.1 and 7.4 ppm).

Temperature reaction modifications do not particularly affect **P1** polymerization. The temperature raising does not modify the backbone enchainment giving rise only to higher yield of a material with lower molar mass (5500 Da at 90°C *vs* 4500 Da at 110°C from MALDI-MS).

Homocoupling reactions in SPC, originating from oligomeric chains having boronic ester end groups, are well known in the literature.[47] When occurring, they involve the incorporation of structural defects in the polymer main chain that cannot be further removed. This deviation from the perfect alternating enchainment can modify the optoelectronic properties of the resulting material as well as their photovoltaic performances. For this reason, it is important to control all the polycondensation conditions to reduce or, better, to fully eliminate these side reactions, thus obtaining homocoupling-free materials.[48]

^{1}H-NMR analyses reveal the amount of Cbz-Cbz homocoupling as a function of the diazine monomer. It is very small in the synthesis of **P1** with $Pd_2(dba)_3$/P(*o*-tol)$_3$ but greatly increases in **P2-run1** (**Fig 2**).

The **P1** ^{1}H-NMR spectrum (**Fig. 2a**) shows the singlet at 9.88 ppm due to the proton on the imine bond (Hd), as well as a broad doublet at 8.45 ppm attributed to carbazole protons Hc. The other broad doublet at 7.50 ppm is attributable to protons Hb belonging to carbazole as well. For protons Ha, two signals are visible and are due to slow rotation of the alkyl chain –$CH(C_8H_{17})_2$ at the N-CH bond, because the two aromatic moieties of the carbazole unit are not equivalent at room temperature.

The set of three small signals at 8.29, 7.75, and 7.63 ppm (highlighted with * in **Fig 2a**) are ascribed to the presence of a small amount of Cbz-Cbz homocoupling in the polymeric backbone of **P1**.[49, 50] MALDI-MS experiments (see below) are in complete agreement with these results and highlight the additional presence of Cbz-Cbz homocoupling already in the starting monomer **12**. As a matter of fact, no signals due to polymer chains containing additional carbazole units than those expected are observed, except those related to chains ending with both carbazole

moieties (compare species A_n *vs* B_n - in **Fig. 5** and **Table S2** in the supplementary material). On the contrary, the ^{1}H-NMR spectrum of **P2** (**Fig 2b**) is clearly representative of an oligomer mixture, because of a huge number of small signals related to both Cbz-Cbz homocoupling and the presence of short chains, depicting different surroundings of thieno[3,4-*d*]pyridazine rings according to their position along the chain (**Fig 2b**, see the inset) detectable in the 9.3-9.9 ppm range. As a matter of fact, MALDI-MS analysis of this sample shows that homocouplings diazine-diazine take place reducing the backbone length (see below MALDI-MS section and **Fig. S3** in the supplementary material).

The use of Pd(PPh3)4 was suitable for the synthesis of **P2** as the thiophene presence makes monomer **M2** less electrophilic than phthalazine. In fact it is more reactive than mixtures of $Pd_2(dba)_3$ and triphenylphosphine towards (*vis à vis)* oxidative addition[51] and might speed the reaction up even if this complex could promote other side reactions as scrambling. The use of toluene as solvent requires biphasic condition where the oxidative homocoupling can frequently occur in the presence of oxygen impurities, hence reaction conditions where a higher concentration of the reactive species $Pd(0)(PPh_3)_2$ was used for this synthesis.

Using $Pd(PPh_3)_4$ as catalyst, the **P2** molar mass average (M_n and M_w) increased reaching values near 4000 Da (determined by MALDI-MS). The increase in the reaction temperature caused the decrease of the Cbz-Cbz homocoupling from ~50% at 90 °C (**P2-run2**), to ~10-15% at 100 °C (**P2-run3**) (**Fig. 3a** and **b**). A further temperature increase gave rise to thienopyridazine-thienopyridazine (Thdz-Thdz) enchainments as revealed by MALDI-MS analysis, which agrees with the decrease in ^{1}H-NMR spectrum of the intensity of carbazole proton signal around 8.15 ppm (Cbz-Cbz homocoupling) and the increase of the thieno[3,4-*d*]pyridazine ones at 9.62-9.65 ppm (**P2-run4**, **Fig. 3c**).

As revealed by MALDI-MS characterization (**Fig. 5, 6, 7**), the increase of the reaction temperature over 100 °C for both **M1** and **M2** monomers led to higher yields but to disordered materials.

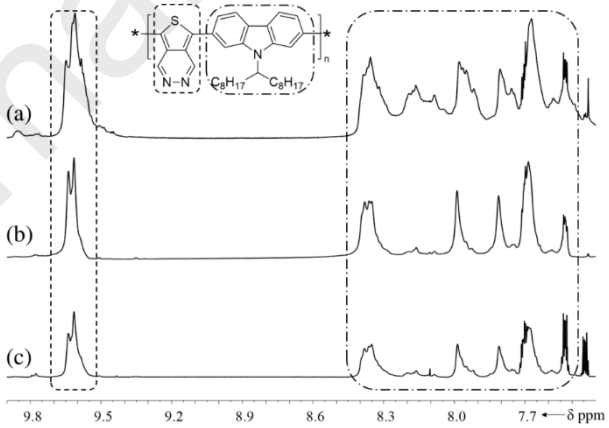

Fig. 3 ^{1}H-NMR spectra of **P2-run2** synthetized at 90 °C (a), **P2-run3** at 100 °C (b), and **P2-run4** at 110 °C (c) in $CDCl_3$, 300K, 400 MHz (expansion in the aromatic region between 7.4 ppm and 9.9 ppm). The dashed area shows the signals assigned to Thdz units, while the dotted-dashed area the signals assigned to Cbz units.

Both the copolymers were further converted into the corresponding metallopolymers **ReP1** and **ReP2**, by refluxing them in toluene solution in the presence of an excess of $Re(CO)_5Cl$ (as sketched in **Scheme 1**). The compounds were

isolated in high yields (~70%) as yellow and dark purple powders for **ReP1** and **ReP2** respectively, by precipitation with *n*-hexane from the corresponding saturated dichloromethane solutions, and their ^{1}H-NMR spectra were measured (**Fig. 4**). **ReP1** is soluble in chloro- and *o*-dichlorobenzene (*o*-DCB), but scarcely in chloroform and tetrahydrofuran, while **ReP2** is slightly soluble and hardly dissolves in hot aromatic chlorinate solvents.

In order to assess the occurrence of the complexation reaction, the amount of Re in **ReP1** and **ReP2** was estimated by inductively coupled plasma atomic emission spectroscopy (ICP-AES) analysis, obtaining 31.7±0.5% and 31.2±0.5% for **ReP1** and **ReP2** respectively, using **P1-run3** and **P2-run3** as starting materials.

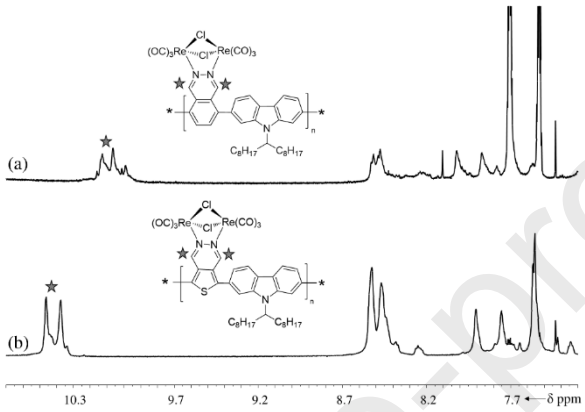

Fig. 4 ^{1}H-NMR spectra of metallopolymers **ReP1** (a) and **ReP2** (b) in CD_2Cl_2, 300K, 400 MHz (expansion in the aromatic region between 10.7 and 7.4 ppm, stars highlight the signals due to the rhenium complexation reaction).

As mentioned above, MALDI-MS spectrometry allows to gain more information on composition, end chain groups, and even microstructure of the polymer chains composing the copolymer backbones, hence MALDI-MS spectra of different runs were collected.

Mass spectra of the **P1-run1** and **P1-run4** copolymers are displayed in **Fig. S1** and **Fig. S2** in the supplementary material, respectively. Both mass spectra show a series of repeating peaks having 531.8 ± 0.3 Da transitions, corresponding to the mass of the repeating unit (Cbz-Phdz) of the copolymer **P1**. The mass spectrum of **P1-run4** (**Fig. 5a**) leads to the identification of 19 clusters of homologous peaks, whereas that of **P1-run1** (**Fig. 5b**) of 18 peak series corresponding to **P1** copolymer chains bearing different end groups. The pertinent structural assignments are summarized in **Table S2** in the supplementary material. In particular, the mass spectrum of **P1-run4** shows two highly intense peaks series: the first attributed to copolymer chains terminated with hydrogen at both ends (family P1-U_n in **Fig. 5a** and in **Table S2**) and the second to copolymer chains terminated with phthalazine and hydrogen (species P1-α''_n in **Fig. 5a** and in **Table S2**). On the other hand, in the mass spectrum of **P1-run1 (Fig. 5b**) two families of peaks appear very intense: the first family belongs to the copolymer chains terminated with hydrogen and carbazole (species P1-B_n), and the second is due to the expected backbones terminated with hydrogen and 5-methylthiophene units (thereafter MeT) (species P1-A_n). This result agrees with the synthetic procedure as 5-methylthiophene borolane derivative was used as the quencher of the reactive bromine ends (**Scheme 1**). However, copolymer chains terminated with bromine were identified in both mass spectra (species P1-A''_n, P1-C'_n, P1-C''_n, P1-Q_n) indicating that an incomplete

end-quenching reaction occurs mostly at 110°C. In fact, these mass peaks are more intense in the mass spectrum of **P1-run4,** while in that one of **P1-run1** the peaks belonging to the copolymer chains terminated with a MeT group (**Fig. 5b**, species P1-A_n, P1-A'_n, P1-C_n, P1-D_n, P1-R_n, P1-γn, P1-γ'n,) prevail.

Both MALDI-MS spectra in **Fig. 5** present less intense peaks corresponding to the families of oligomers having palladium and/or phosphorus derivatives (species P1-ϱ_n, P1-ψ_n, P1-δ_n, P1-φ_n, P1-ε_n), as already observed in the characterization of copolyfluorenes synthesized by Suzuki coupling reaction.[52]

Furthermore, the mass spectra show unequivocally the formation of some Cbz-Cbz dyads (species P1-D_n, P1-L_n, P1-γn, P1-γ'n, P1-βn, P1-β'n, in **Fig. 5** and **Table S2**) and of Phdz-Phdz dyads (species P1-ε_n, in **Fig. 5** and **Table S2**), owing to the homocoupling reactions occurring during the SPC process, in agreement with the ^{1}H-NMR results. The identification of copolymer chains terminated with hydrogen, hydroxyl, carbazole, and phthalazine units (*i.e.* families P1-A_n, P1-A'_n, P1-A''_n, P1-B_n, P1-D_n, P1-L_n, P1-F_n, P1-Q_n, P1-R_n, P1-U_n, P1-ϱ_n, P1-α_n, P1-α'_n, P1-α''_n, P1-β_n, P1-β'_n, P1-χ'_n, P1-φ_n, P1-ε_n in **Fig. 5** and **Table S2**) clearly confirms , as already reported in the literature,[52-56] the occurrence of side reactions (such as debromination, hydrolytic deboronation, hydroxy deboronation) in the SPC between dibromide and diborolane monomers. Since the mass spectra of **P1-run2** and **P1-run3** (not reported here for the sake of brevity) are remarkably similar to that of **P1-run1**, from the MALDI-MS analysis it emerges that the debromination and hydrolytic deboronation side reactions prevalently occur at 110°C.

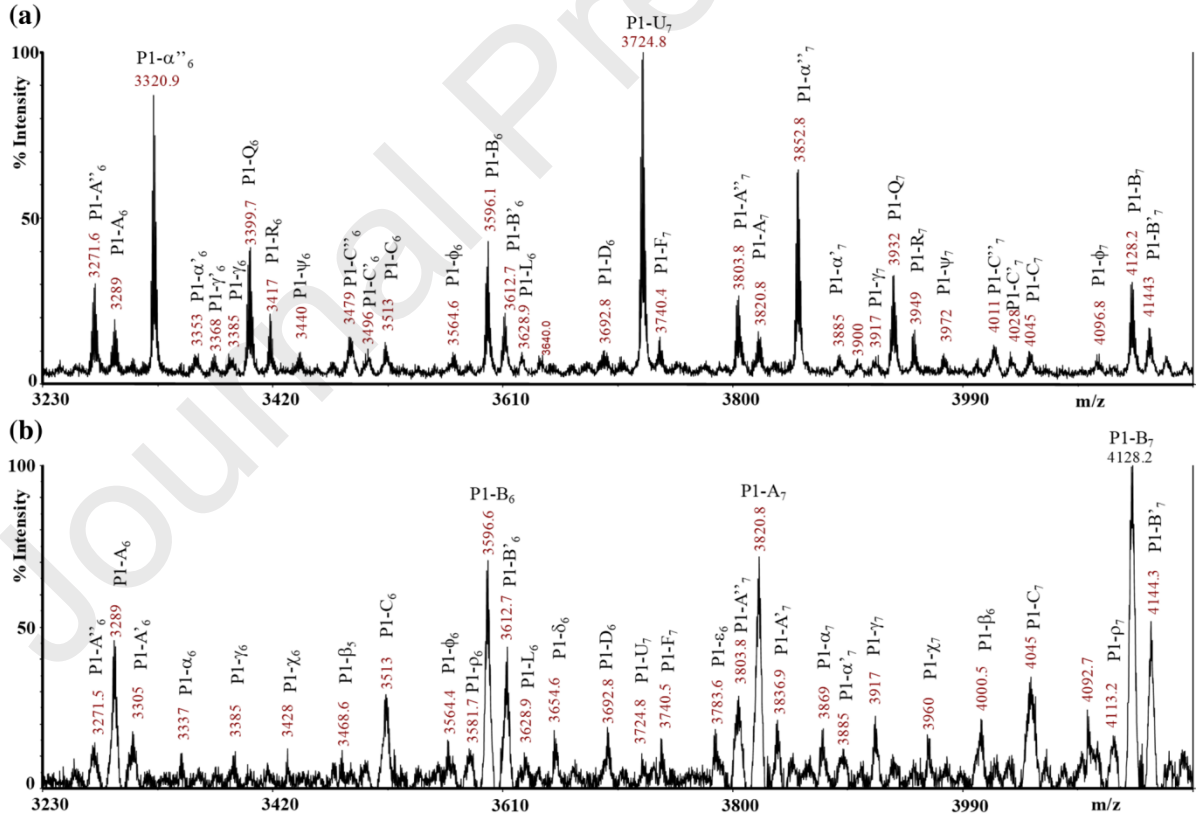

Fig. 5 Enlarged section of MALDI-TOF mass spectra of **P1** samples in mass range between 3230 – 4150 m/z: (a) **P1-run4**; (b) **P1-run1**, recorded in reflectron mode using DCTB as the matrix.

Like **P1, P2** was characterized through MALDI-MS, and the obtained data are reported in **Table 2**. Mass spectrum of **P2-run1** (**Fig. S3** in the supplementary material), synthesized via the protocol used for **P1** samples, shows extremely low MM oligomers (dimers and trimers) bearing different end groups (see assignments in **Table S3** in the supplementary material). It also shows the presence of unreacted dibolorane carbazole derivative constituted by Cbz-Cbz dyad (peaks at m/z 657.9) and Cbz-Cbz-Cbz triad end (peaks at m/z 1061.3; see inset of **Fig. S3**). These reactive macromers are present in the crude parent monomer used in the synthesis of **P2-run1**, as confirmed by MS analysis. Oligomers containing the above Cbz-Cbz dyads (peaks labelled with the symbols ◊, ε, τ, τ′, □, η) and Cbz-Cbz-Cbz triads (peaks labelled with the symbols □, π, θ, ψ, ∇) were also detected. The assignments of the representative peaks in the mass spectrum reported in **Fig. S3** and noted in **Table S3** reveal that the oligomers containing Thdz-Thdz homosequences are formed too. Furthermore, **Table S3** indicates that oligomers terminated with reactive bromine and/or borolane groups are formed as well as ones containing unreactive end groups (MeT, H, OH, thieno[3,4-*d*]pyridazine, carbazole). Moreover, short copolymer chains containing Pd catalyst were also detected. As reported above, the synthesis of the other **P2** copolymers was carried out exploiting $Pd(PPh_3)_4$ as the catalyst instead of $Pd_2(dba)_3/P(o\text{-tol})_3$ previously used (**Table 1**). The mass spectra of the **P2-run2**, **P2-run3**, and **P2-run4** in the mass range between 1587 and 2580 m/z are reported in **Fig. 6**, while **Fig. 7** shows the mass spectra of the **P2-run3** and **P2-run4** in the mass range from m/z 2880 up to 3480, and the assignments are summarized in **Table S4** in the supplementary material. Total MALDI-MS spectra of **P2-run2**, **P2-run3**, and **P2-run4** are displayed in **Fig. S4**, **Fig. S5**, and **Fig. S6** in the supplementary material, respectively.

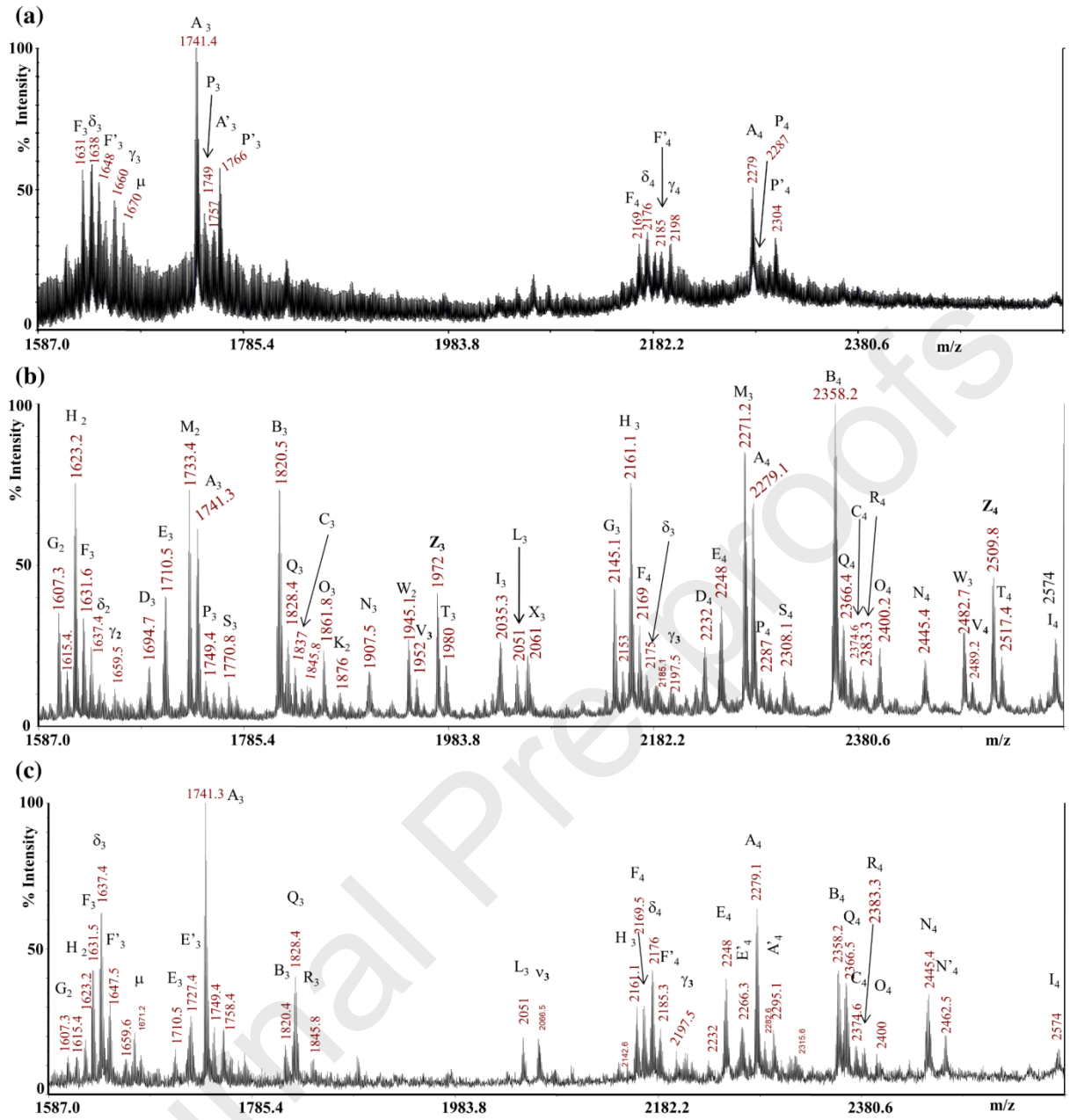

Fig. 6 Enlarged section of the MALDI-TOF mass spectra of the **P2** oligomers (a) **P2-run2**, (b) **P2-run3**, (c) **P2-run4** in the mass range between 1587 and 2580 m/z, recorded in reflectron mode using DCTB as the matrix.

More complicated mass spectra were recorded for **P2-run3** and **P2-run4** with respect to that of **P2-run2**, as observed in **Fig. 6**. 9 families of P(Cbz-Thdz) oligomers bearing different chain ends were revealed after purification of **P2-run2**, whereas 18 and 26 species were seen for purified **P2-run3** and **P2-run4** respectively (**Fig. 6**). The most intense peak family in the mass spectrum of **P2-run2** (**Fig. 6a**) corresponds to the expected coupling P(Cbz-Thdz) for **P2** oligomers, terminated with reactive borolane group to one end, and hydrogen to the other (species A_n in **Table S4**). Oligomers terminated with thienyl[3,4-d]pyridazine unit (Thdz) at both ends (species P_n), were also observed, while the peak series F_n corresponds to the oligomers terminated with H and OH. The mass spectra in **Fig. 6a** and **Fig. S4** are representative of the purified **P2-run2**, after filtration through

a diatomaceous earth pad. However, since a low yield was obtained (>30%) in this run, we can suppose that a large amount of copolymer was retained on the inorganic pad. The purification procedure was optimized in the next runs to completely wash the pad and to increase the yield (**Table 1**). Although this fact does not affect the evaluation of the different enchainment in the polymer backbones, a modified purification procedure was applied to **P2-run3** and **P2-run4**, leading to good yields (~60 %, **Table 1**), therefore the mass spectra of these samples **(Fig. 6b-c** and **Fig. 7**) should be more representative of the chemical composition of these copolymers. In both samples, P(Cbz-Thdz) oligomers terminated with the reactive borolane and bromine groups were identified, and with unreactive moieties (MeT, hydrogen, hydroxyl, Cbz, and Thdz units, see **Table S4**) as expected for the polycondensation and the side reactions (debromination, hydrolytic deboronation, hydroxy deboronation) occurring during the synthetic procedures. P(Cbz-Thdz) oligomers terminated with the reactive borolane group (species A_n, B_n, H_n and M_n, **Table S4**) give the most intense peak families in the mass spectra of the **P2-run4** **Fig. 6c** and **Fig. 7b**). Like for the other samples (all **P1** samples and **P2-run1**), the P(Cbz-Thdz) oligomers containing palladium and/or phosphorus derivatives (*i.e.* species δ_n, γ_n, μ_n, W_n, υ_n, Pd_n, Pd'_n, Pd''_n, **Table S4**), were also observed. Furthermore, in the case of **P2-run4** mass spectrum, the formation of copolymer chains bearing Thdz-Thdz homosequences (Thdz-Thdz dyads, *i.e.,* species T_n, V_n, Z_n, δ_n, γ_n, Pd''_n, in **Fig. 6c** and **Fig. 7b**, and in **Table S4**), due to homocoupling reaction was also detected.

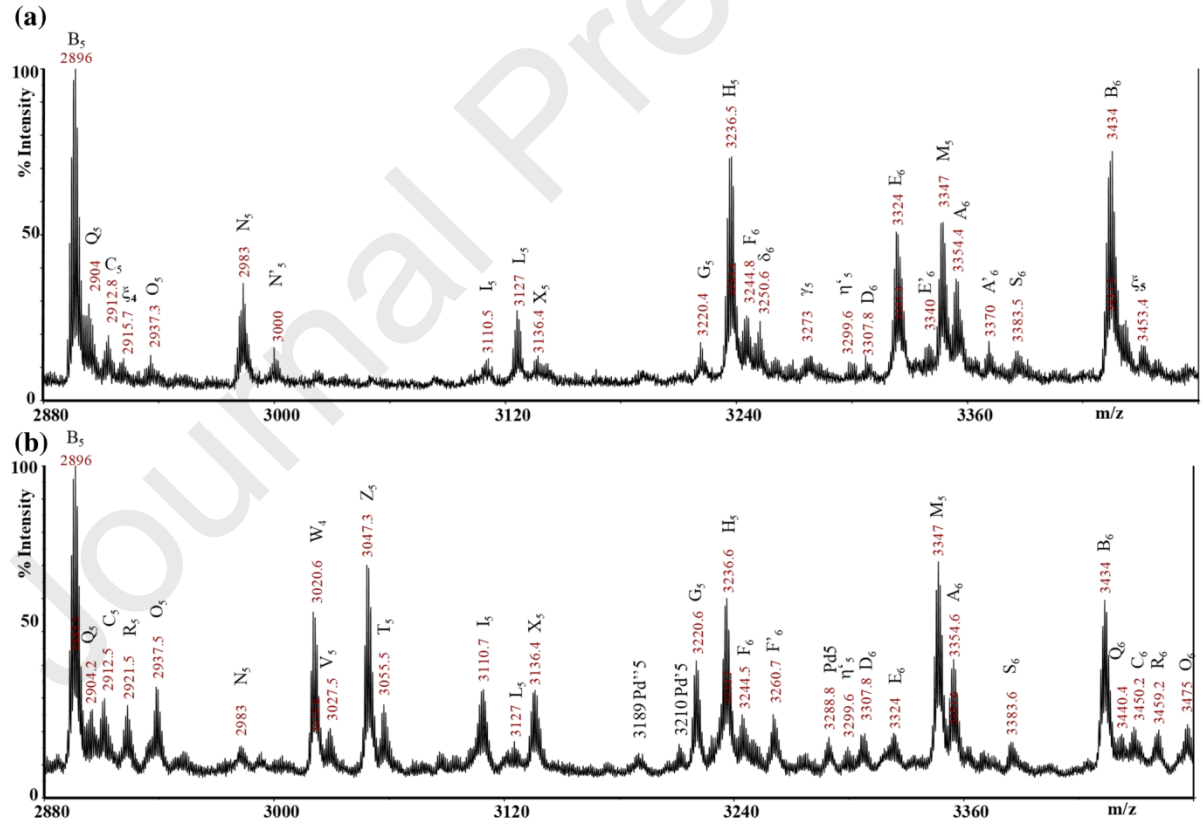

Fig. 7 A section of the MALDI-TOF mass spectra of the **P2** oligomers: (a) **P2-run3**, (b) **P2-run4** in the mass range between 2880 and 3470 m/z, recorded in reflectron mode using DCTB as the matrix.

The species Z_n containing Thdz-Thdz dyads along the chains give very intense

peaks in the mass spectra of **P2-run4** (**Fig. 6c** and **Fig. 7b**). Since the Thdz-Thdz dyads were not observed in the **P2-run3** synthesized at 100 °C, we conclude that the Thdz-Thdz homocoupling reaction occurs at temperature higher than 100°C. Therefore, the alternate and homogeneous P(Cbz-Thdz) copolymers can be mostly synthesized at 100 °C.

The molar mass distribution (MM; Mw, Mn, and Mw/Mn) of **P1** and **P2** was calculated by the MALDI-MS recorded in linear mode by means of the Data explorer software applying the Polymer Analysis Toolbox, and the results are reported in **Table 2**.

Table 2 Molar mass distribution of **P1** and **P2** calculated by MALDI-MS recorded in linear mode.

sample	M_n [Da]	M_w [Da]	M_w/M_n
P1-run1	5500	6450	1.17
P1-run4	4500	5210	1.14
P2-run1	1220	1815	1.49
P2-run2	3180	4170	1.31
P2-run3	4070	4830	1.18
P2-run4	3930	4600	1.17

The molar mass determination was performed by SEC tools to calculate molar mass averages (M_n, M_w) and the polydispersity index M_w/M_n. Different conditions were tested for the analysis and in particular different eluents were used in order to reduce the strong interaction between the column stationary phase and the imine nitrogen electron lone pair. The values obtained for the samples **P1-run4** and **P2-run4** are reported in **Table S1** in the supplementary material. They are very far from those obtained from MALDI-MS. The impossibility of carrying out molar mass characterization using only chloroform as the eluent, differently from what observed by Gendron *et al.*[6] for materials having comparable masses, indicates a higher nucleophilic character of the fused 1,2 diazine when it is in side position rather that in the conjugated backbone.

Indirect evidence on the formation of both metallopolymers (**ReP1** and **ReP2**) was also obtained by MALDI-MS analysis, since the mass spectra of these samples show signals due only to the clusters of the matrix with the $Re(CO)_3$ moiety (**Fig. S7**). This behaviour was observed with all matrixes used.

All polymers and metallopolymer samples were characterized by means of differential scanning calorimetry (DSC). The materials are amorphous. As an example, **Fig. S8** in the supplementary material reports the thermogram of the **P1-run1**, and **Fig. S9** that one of the corresponding **ReP1**. A qualitative comparison of the thermograms of the metallopolymer samples with those of the corresponding starting polymers was possible and some differences are detectable that could be associated with formation of the Re-diazine complexes along the polymer chains.

Theoretical calculations, spectroscopic and electronic characterization. Density functional theory (DFT) geometry and time-dependent DFT (TD-DFT) calculations of the absorption spectra in dichloromethane (see the

supplementary material for a full discussion) were performed to assess the structural features of the examined compounds and to provide a definite assignment of the observed electronic transitions. The calculations were carried out on both the perfectly alternating tetrameric units $(Cbz\text{-}Phdz)_4$, $(Cbz\text{-}Thdz)_4$, $(Cbz\text{-}RePhdz)_4$, and $(Cbz\text{-}ReThdz)_4$, simulating the regular polymeric chains, and the defective tetrameric models with either Phdz-Phdz/Thdz-Thdz or Cbz-Cbz homocoupling. The spectroscopic data of the polymers **P1**, **P2** and the corresponding metallopolymers **ReP1** and **ReP2**, recorded in dichloromethane solution, are summarized in **Table 3**.

Table 3 Spectroscopic data including the wavelength of the maximum absorption peaks for the different transition bands ($\lambda_{\pi\text{-}\pi^*}$, $\lambda_{IL(+ML)CT}$, $\lambda_{MLCT,\ and}$ λ_{ILCT}), the wavelength of the maximum of the emission band (λ_{em}) and the photoluminescence quantum yield (ϕ) of the different species in diluted dichloromethane solution at room temperature.

sample	$\lambda_{\pi\text{-}\pi^*}$ [nm] ($\varepsilon\cdot10^4$)	$\lambda_{IL(+ML)CT}$ [nm] ($\varepsilon\cdot10^4$)	λ_{MLCT} [nm] ($\varepsilon\cdot10^4$)	λ_{ILCT} [nm] ($\varepsilon\cdot10^4$)	λ_{em} [nm]	Φ [%]
P1	266 (1.60)		-	366, 370 (1.55)	450	11.0
P2	262 (2.27)	344 (1.02)	-	461 (1.05)	572	10.1
ReP1	273 (5.79)	312 (2.6)	385 (2.44)	424 (2.35)	614	3.0
ReP2	274 (3.31)	362 (1.59)	388 (1.18)	554 (0.80)	670	5.8

The absorption spectra of **P1** and **P2** in dichloromethane solution are displayed in **Fig. 8** while **Fig. S10**, **Fig. S11** and **Table S5** in the supplementary material show the absorption spectra and the band assignment computed for the models. Both the polymer spectra display a high energy band, centered at about 260 nm for **P1** and about 270 nm for **P2**. We attribute it to the π-π^* transition of the conjugated backbone from HOMO-1 (**P1**) or HOMO (**P2**) to high-lying LUMO+8, LUMO+9 (**P1**) or LUMO+6 (**P2**) (**Fig. S12** in the supplementary material).

In the lower energy part of the spectrum, **P2** shows two main absorption bands at 461 and 344 nm (**Fig. 8b**), both having partial charge transfer (CT) character from the π-delocalized system of the backbone to π^* orbitals mainly localized on the pyridazine unit. Though such CT contribution is hardly discernable from mere visual inspection of the highest occupied molecular orbital (HOMO) and lowest unoccupied molecular orbital (LUMO) (**Fig. 9**) mainly involved in this transition (81%), the D-A character of the Cbz-Thdz-Cbz subunit is clearly manifested by its large dipole moment (6.92 D) and the electrostatic potential map (**Fig. S13** in the supplementary material).

Concerning the characterization of possible homocoupling defects in **P2**, TD-DFT calculations on either the perfectly alternating tetramer $(Cbz\text{-}Thdz)_4$ or on the defective models with Cbz-Cbz or Thdz-Thdz homocoupling provide low energy bands at 502, 482 and 562 nm, respectively (**Fig.s S14-S17** and **Table S6** in the supplementary material). Based on these results, comparison among the spectra of **P2** as obtained in three different synthetic conditions (**Fig. 8c**) suggests that Thdz-Thdz homocoupling defects can be safely excluded in **P2-run2** and **P2-run3**, while occurring in **P2-run4**. In the **P2-run4** spectrum an extended red-shifted absorption was observed as shoulder of the band at 460 nm. Cbz-Cbz homocoupling

could instead be present in **P2-run2**, whose low energy band is blue-shifted by about 20 nm with respect to that of **P2-run3**. The blue-shift of **P2-run2** partially reduces the anomalous disagreement in the position of this band as computed for the perfectly alternating tetramer and that observed in the experimental one (502 *vs*. 460 nm, respectively).

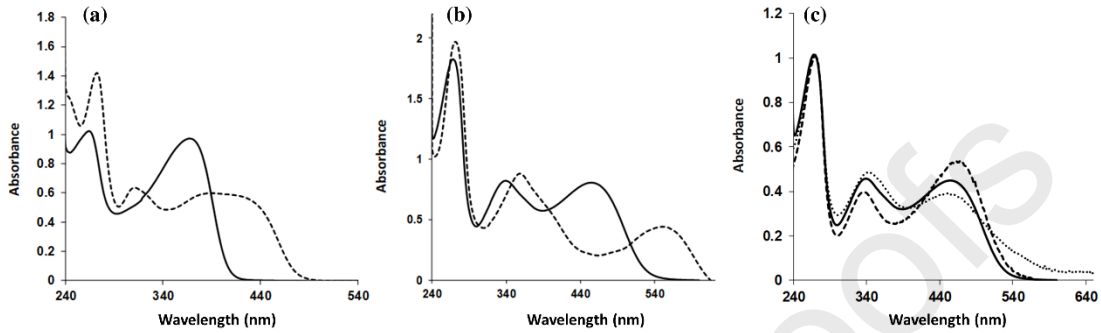

Fig. 8 Absorption spectra in CH_2Cl_2 at room temperature of (a) **P1** (solid line) and the corresponding **ReP1** (dotted line); (b) **P2** (solid line) and the corresponding **ReP2** (dotted line); (c) normalized absorption spectra of **P2-run2** (solid line), **P2-run3** (dashed line) and **P2-run4** (dotted line). All spectra were measured in dichloromethane solution at room temperature.

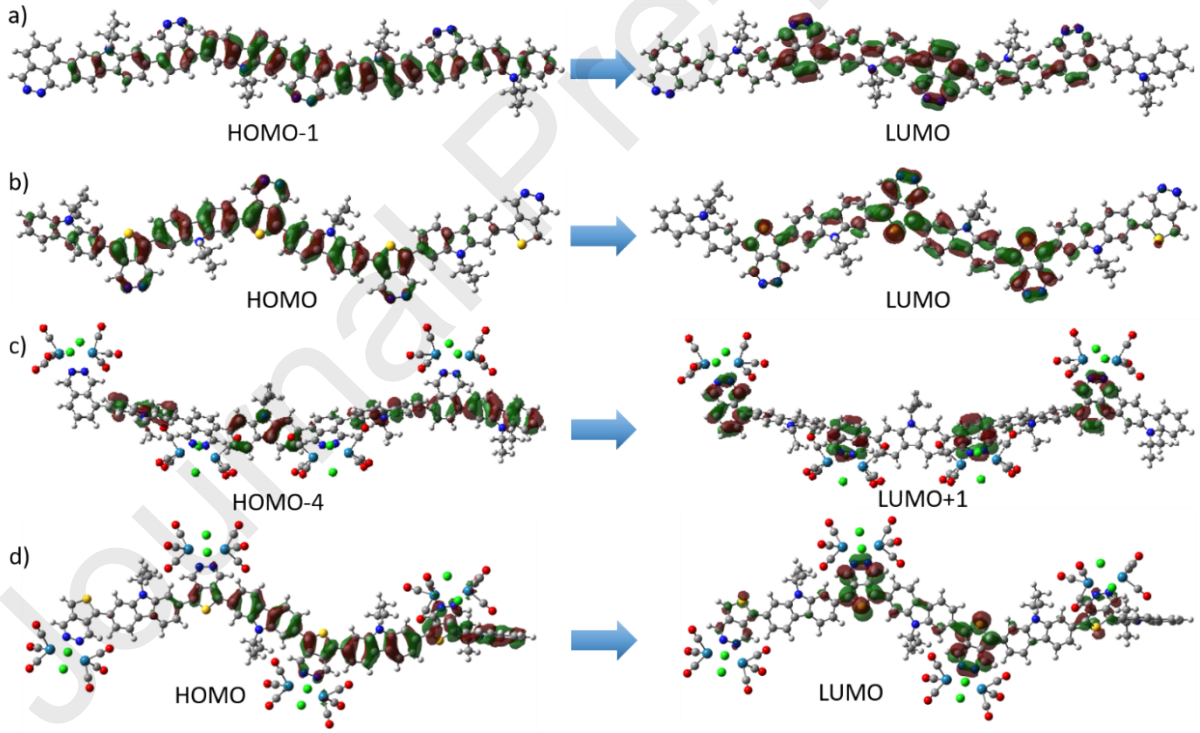

Fig. 9 Isodensity surface plot of the (PCM)TD-PBE0/SVP frontier orbitals of tetramers $(Cbz\text{-}Phdz)_4$ (a), $(Cbz\text{-}Thdz)_4$ (b), $(Cbz\text{-}RePhdz)_4$ (c) and $(Cbz\text{-}ReThdz)_4$ (d), mainly involved in the lower energy transitions (isosurface values: 0.02).

Differently from **P2**, polymer **P1** shows in its UV spectrum only one broad absorption band centered at about 370 nm (**Fig. 8a**) due to CT transition involving the π-delocalized system of the backbone and the π^* orbitals localized on the Phdz moiety (**Fig. 9**). Similar to **P2**, the CT character is provided by the D-A nature of the constituting units, with the pyridazinic nitrogen atoms acting as strong electron-

withdrawing group (**Fig. S13** in the supplementary material for the electrostatic potential map of Cbz-Phdz-Cbz, having dipole moment equal to 6.57 D). The observed blue-shift of the CT band in **P1** compared to the same band in **P2** can be explained by analyzing the frontier orbitals of the two compounds. According to DFT calculations (**Table S6** in the supplementary material), the LUMO and the HOMO of $(Cbz\text{-}Phdz)_4$ are respectively higher and lower in energy than those of $(Cbz\text{-}Thdz)_4$, so that a larger HOMO-LUMO energy gap is computed for the former (ΔE = 3.87 eV) than the latter (ΔE = 3.04 eV). The energy decrease of the HOMO is due to the stronger electron-donating character of the thienylene unit in Thdz compared to that of the phenylene unit in Phdz. The thieno[3,4-*b*]pyrazine ambipolar character reported by Rasmussen and coworkers[7, 57] leads to the hypothesis that in the **P2** backbone only the pyridazine ring in Thdz moiety behaves as an acceptor unit.

The spectra of both **P1** and **P2** are significantly perturbed upon metal coordination, although in different ways. In the **ReP2** spectrum, a significant bathochromic shift of the CT bands (from 461 and 344 in **P2** to 554 and 362 nm in **ReP2**, **Fig. 8b**) is observed, due to the stabilization of the LUMO level upon coordination to metal centers. Moreover, the presence of the "$Re(\mu\text{-}Cl)_2Re$" moiety introduces a further electronic transition giving rise to a partial metal-to-ligand charge transfer (MLCT) character to the higher energy ligand centered or to the intraligand charge transfer (ILCT) transition. The mere MLCT transition from the $d\pi$(Re) orbitals of the metal center to the Thdz π^* orbital is instead observed as a shoulder at 388 nm. The same MLCT absorption band is observed also in the **ReP1** spectrum (385 nm), while the mixed MLCT/ILCT and the ILCT absorption bands lie at 312 and 424 nm, respectively. From these results, we can conclude that the band gap of the metal free conjugated polymer **P2** can be significantly reduced by introducing the rhenium(I) moieties into the polymer backbone, making this metallopolymer a promising photosensitizer for OPV cells. Hence, according to **Fig. 8**, the absorption range is extended by 100 nm into the red down to 640 nm, like that of the extensively-used poly(3-hexylthiophene-2,5-diyl) (P3HT) polymer.

Upon optical excitation, all the polymers and the corresponding metallopolymers are luminescent in the visible range of the electromagnetic spectrum. The photophysical data are reported in **Table 3**. It is interesting to note that emission of **P1** is strongly blue-shifted with respect to the emission of **P2**, in agreement with the higher energy gap obtained from the DFT calculations. The coordination to the metal center strongly quenches the emission intensity and causes a bathochromic shift of the emission maximum of more than 100 nm for both the polymers. This behavior is attributable to the occurrence of a low energy ^{3}MLCT excited state, which decays in a radiative way as usually observed in closely related dinuclear rhenium complexes.[35, 36]

Energy levels are crucial for the selection of appropriate materials acting as electron donors in bulk heterojunction solar cells. The HOMO and the LUMO energy levels of the polymers and their corresponding metallopolymers were evaluated by CV carried out in nitrogen-saturated acetonitrile, as reported in the supplementary material,[58] and the calculated HOMO and LUMO energy values are reported in **Table 4**.

Table 4 First reduction and oxidation peak potentials, electrochemical (ΔEe) and spectroscopic (ΔEs) energy gaps and energy levels of the frontier orbitals of the polymers **P1**, **P2**, **ReP1** and **ReP2**.[a]

sample	E_{red} [V]	E_{ox} [V]	λ_{abs} [nm]	E_{LUMO} [eV]	E_{HOMO} [eV]	ΔE_e [eV]	ΔE_s [eV]
P1	-1.86[b]	1. 77[b]	376	-2.54	-6.17	3.63	3.30
P2	-1.56 (-1.90)	1.62 (1.47 onset)	460	-2.87	-5.87_{onset}	3.00	2.70
ReP1	-1.20	1.65 (1.47 onset)	385-430	-3.20	-5.87_{onset}	2.67	2.88
ReP2	-0.85 (-1.32)	1.68 (1.44 onset)	554	-3.55	-5.84_{onset}	2.29	2.24

[a] Potentials are referred to the SCE electrode in the operating medium (CH_2Cl_2 + 0.1 M $[NBu_4][PF_6]$). Scan rate 0.2 V s^{-1}. [b] Scan rate 50 mVs^{-1}

As shown in **Fig. 10**, **P1** exhibits a reversible monoelectronic reduction wave, which is located on the Phdz ligand, as indicated by the modulation of the peak potential. **P1** displays a more negative reduction potential than that observed for **P2** (-1.86 V *vs* -1.53 V), in agreement with the lower aromatic delocalization between the benzene ring and the two lateral carbazole rings. The presence of a partial delocalization shifts the reduction peak of **P1** at slightly higher potential than that observed for the bare Phdz ligand (2.07 V *vs* SCE).[27]

The coordination to the metal centers provides a further shift of the reduction potential to more positive values as already observed in analogous complexes.[35] Therefore, the reduction peak shifts to -1.20 V (reversible) and -0.85 V for **ReP1** and **ReP2**, respectively. Moreover, **ReP2** displays a second reduction peak at -1.32 V (partially reversible) whose intensity depends on the sample run. It prevails in the metallopolymer obtained from **P2-run2**, whilst for the metallopolymer obtained from **P2-run4** the two reduction peaks are comparable in intensity in the CV trace. These double reduction peaks could be related to the presence, along the polymer backbone, of two different diazine moieties. In particular, those bounded to Cbz units display a reduction peak at -0.85 V, whose intensity increases in the CV trace of the polymer characterized by Cbz-Cbz homocouplings such as in **P2-run2,** as revealed from MALDI-MS analysis. On the contrary, the Re-diazine units bounded to Thdz units display a more negative reduction peak (-1.32 V) whose intensity increases in the polymers affected by large Thdz-Thdz homocoupling, as in **P2-run4**.

In the anodic part of the CV scan, a bi-electronic oxidation peak is observed at about 1.6 V for **ReP1** and **ReP2**. This peak is attributed to the oxidation of the metal center, in agreement with that observed for analogous complexes. The intense oxidation of the metals partially covers the oxidation peak of the polymeric backbone, which is observed at lower potential. The more conjugated (Cbz-Thdz) moiety in **P2** displays a lower oxidation potential than that observed for the (Cbz-Phdz) unit in **P1** (1.77 V *vs* 1.44 V for the onsets). The modulation of the potential of the first oxidation peak, upon changing the size of the central aromatic ring, supports this hypothesis.

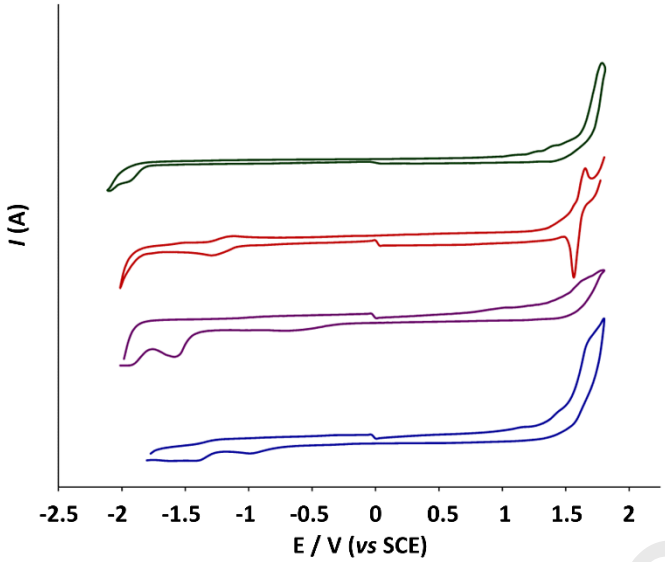

Fig. 10 CV features obtained for P2 (purple) and the metallopolymers ReP1 (red) and ReP2 (blue) at 0.2 $V \cdot s^{-1}$ scan rate, in acetonitrile, with 0.1 M $TBAPF_6$ as supporting electrolyte, at 298 K, with GC as working electrode. For P1 (green) the CV characteristic is obtained at 50 mV/s in order to observe the oxidation peak in the available potential window. All the curves are normalized for the scan rate.

Device Fabrication and characterization. Polymer solar cells were fabricated using [6,6]-phenyl-C61-butyric acid methyl ester (hereafter PCBM) as acceptor material, blended with the different molecules synthesized in this work as donor materials of the active layer (with a blend ratio of PCBM:donor=2:1). Taking into account the structural characterization of the materials, **P1-run4** and **P2-run3** were used for the preparation of the device, as they showed a lower number of defects in the alternation of the electron donor/acceptor monomers along the polymeric backbone. The **ReP1** and **ReP2** metallopolymers used for the device fabrication were prepared from **P1-run4** and **P2-run4**, respectively. The latter was chosen to investigate the effect of a large presence in the donor material of Thdz-Thdz homosequences. The solar cells were prepared in a single layer direct architecture using PEDOT:PSS as hole transport layer and calcium as top contact selected for their charge-collecting properties[59, 60], with different donor polymers and their rhenium complexes for the photoactive layer (thickness of ~200 nm) annealed at 120 °C. No addictives, such as 1,8-diiodooctane for example, were used during the fabrication of the devices.[61] The current density-voltage curves of PCBM:donor solar cells with the different donor materials under 1 sun irradiation, and the corresponding curves in the dark were reported in Fig. S18 in the supplementary material. The PV parameters of the cells for different donor polymers, **P1**, **ReP1** and **P2**, **ReP2**, annealed at 120 °C are reported in **Table 5** and **Table S7,** respectively.

Table 5 Averages[a] of the PV parameters of direct architecture solar cells annealed at 120 °C.

Device [b]	J_{sc} [mA/cm2]	V_{OC} [V]	FF [%]	PCE [%]
P1	0.02 ±	0.265 ±	39.64 ±	0.002 ±

	0.002	0.046	10.6	0.0001
ReP1	0.06 ± 0.005	0.557 ± 0.011	33.11 ± 5.40	0.011 ± 0.0001

[a] six devices were tested; [b]active layer: blend PCBM:donor=1:2. Reference blend PCBM:P3HT=1:1 in direct solar cell devices, annealed 130 °C, J_{sc}=7.87±0.75 mA/cm²; V_{oc}=565±5 mV; FF=48.19±0.07%; PCE=2.14±0.18 %.

Whereas the performance is extremely low for both **P1** and **P2** polymers, performance improves an order of magnitude at the same processing conditions when metallopolymers **ReP1** and **ReP2** are used. This improvement is not only due to higher photocurrents consistent with lower energy gaps but also to larger V_{OC} values.

It is possible to compare these data with those reported in literature[42-44] and obtained from the measurement with poly[*N*-(9-heptadecanyl)carbazole-2,7-diyl-*alt*-benzo-2,1,3-thiadiazole-4,7-diyl) (PCbzBT), a copolymer bearing a 2,1,3-benzothiadiazole unit in place of the diazine monomers used in this work, performed on a direct architecture PV cell fabricated in comparable conditions. It is possible to observe a higher photocurrent and power conversion efficiency with respect to the values obtained for **P1** and **P2**, respectively (PCE = 1.5% *vs* 1.1x10^{-2}% for **P1** and 0.2x10^{-2}% for **P2**).[42, 62]

A further comparison is possible with the copolymer poly(*N*-(2-ethylhexyl)carbazole-3,6-diyl-*alt*-(2,3-dimethyl)thieno[3,4-*b*]pyrazine-5,7-diyl) (PCTP) containing *N*-(2-ethylhexyl)carbazole and 2,3-dimethylthieno[3,4-*b*]pyrazine as comonomers for which V_{OC} = 0.33 V, J_{SC} = 0.48 mA/cm², FF = 0.37, and PCE = 0.06% were reported.[63] 2,1,3-benzothiadiazole and 2,3-dimethylthieno[3,4-*b*]pyrazine have a higher electron affinity than those of phthalazine and thieno[4,5-d]pyridazine used in this work that lead to the fabrication of devices with higher V_{OC} totally justifying the observed results. The low PCE values of the polymer-based devices may be due to low absorptivity of the ILCT transition in the visible range compared to the π-π^* transition in the ultraviolet region (2.27x10^4 *vs* 1.05x10^4 for **P2**, both low around 1.5x10^4 for **P1**) well below 10^5 value considering the minimum for good performance.[64] The absorptivity increases by complexation with rhenium and device performance increases too. Overall low efficiency could also be related to the high energy LUMOs of materials containing weak withdrawing 1,2-diazine moiety which strongly affect light harvesting capability (due to an overly large gap) as well as charge photogeneration and dissociation resulting in very low J_{SC}.[64, 65] What is noteworthy is that the absorptivity increases upon complexation, which was not observed for the mononuclear rhenium octahedral complexes already used for photovoltaic applications.[66] The absorptivity increase in the visible region together with a reduction of the energy band gap can explain the increase of J_{SC} in the devices with metallopolymers while the higher energies of the HOMO levels of the complexes make these values nearer to the optimal value of 5.4 eV.[64] Unfortunately, the difficulty in dissolving the metallopolymers into the halogenated solvents used for the deposition of the active layer justify the low value observed for the FF. This observation suggests that charge transport is hindered as well as recombination increased in the devices, probably due to the formation of large aggregates decreasing film homogeneity, that increases phase separation between the donor materials and PCBM, thus leading to low efficiency.[34] Maybe a compromise

related to the amount of the rhenium complex introduced in the materials could be useful to improve performance.

3. Conclusions

The synthesis of two copolymers of 9-(heptadecan-9-yl)-2,7-bis(4,4,5,5-tetramethyl-1,3,2-dioxaborolan-2-yl)-9*H*-carbazole with two different dibromo-1,2-diazines was here reported. Their molecular structure was investigated in depth using ^{1}H-NMR and MALDI-MS techniques. The latter one contributes significantly to determine the enchainment defects in the backbone of both poly[*N*-(9-heptadecanyl)carbazole-2,7-diyl-*alt*-phthalazine-5,8-diyl] and poly[*N*-(9-heptadecanyl)carbazole-2,7-diyl-*alt*-thieno[3,4-*d*]pyridazine-5,7-diyl], **P1** and **P2** respectively. While **P1** shows, substantially, regular enchainment, both carbazole-carbazole and diazine-diazine homocouplings were revealed in **P2** even if a different catalytic system and a larger range of reaction temperatures were explored. The best result (the lowest amount of Cbz-Cbz and no Diaz-Diaz homocoupling detected by MALDI-MS) was obtained using $Pd(PPh_3)_4$ in toluene at 100 °C. As already observed for other carbazole-based copolymers, for example the well-known copolymer PCDTBT, these defects have serious consequences on the electronic properties of the materials as underlined by the spectroscopic and cyclovoltammetric characterizations, corroborated by DFT and TD-DFT calculations. The photoluminescence quantum yield of both **P1** and **P2** is low (11% and 10% respectively), as well as the performance of the materials measured in single layer organic photovoltaic cells due to low absorptivity in the visible range. The increase of the absorbance after the preparation of the corresponding dinuclear rhenium-based metallopolymers **ReP1** and **ReP2** (whose deep characterization is reported), contributes to improved efficiency of the corresponding solar cells. Unfortunately, the two metallopolymers are scarcely soluble causing difficult charge transport to the electrodes and an increased recombination in the active layer.

Author Contributions

The manuscript was written through contributions of all authors. All authors have given approval to the final version of the manuscript.

Declaration of Competing Interest

The authors declare that they have no known competing financial interests or personal relationships that could have appeared to influence the work reported in this paper.

Acknowledgments

This work was financially supported by the National Council of Research (CNR) of Italy and the Ministry of University and Scientific Research (MIUR) of Italy. The work was supported with contribuite of the Italian Ministero degli Affari Esteri e della Cooperazione Internazionale (MAECI), Direzione Generale per la Promozione del Sistema Paese. The Italian Project PRIN 2012A4Z2RY - Aqueous processable polymer solar cells: from materials to photovoltaic modules (AQUA-SOL) is gratefully acknowledged.
The authors wish to thank Dr. R. Mendichi, and Mr. D. Piovani for the structural characterization of the polymers by GPC instrument and the fruitful discussion.

Data availability

The raw data required to reproduce these findings cannot be shared at this time as the data also forms part of an ongoing study. The processed data required to reproduce these findings cannot be shared at this time as the data also forms part of an ongoing study.

References

[1] A. Nitti, G. Forti, G. Bianchi, C. Botta, F. Tinti, M. Gazzano, N. Camaioni, R. Po, D. Pasini, Anthradithiophene-based organic semiconductors through regiodirected double annulations, Journal of Materials Chemistry C 9(29) (2021) 9302-9308.
[2] M. Penconi, G. Bianchi, A. Nitti, A. Savoini, C. Carbonera, D. Pasini, R. Po, S. Luzzati, A Donor Polymer with a Good Compromise between Efficiency and Sustainability for Organic Solar Cells, Advanced Energy and Sustainability Research 2(11) (2021) 2100069.
[3] A. Nitti, P. Osw, G. Calcagno, C. Botta, S.I. Etkind, G. Bianchi, R. Po, T.M. Swager, D. Pasini, One-Pot Regiodirected Annulations for the Rapid Synthesis of π-Extended Oligomers, Organic Letters 22(8) (2020) 3263-3267.
[4] A. Mishra, C.-Q. Ma, P. Bäuerle, Functional Oligothiophenes: Molecular Design for Multidimensional Nanoarchitectures and Their Applications, Chemical Reviews 109(3) (2009) 1141-1276.
[5] R.P. Ortiz, J. Casado, V. Hernández, J.T.L. Navarrete, J.A. Letizia, M.A. Ratner, A. Facchetti, T.J. Marks, Thiophene–Diazine Molecular Semiconductors: Synthesis, Structural, Electrochemical, Optical, and Electronic Structural Properties; Implementation in Organic Field-Effect Transistors, Chemistry – A European Journal 15(20) (2009) 5023-5039.
[6] D. Gendron, P.-O. Morin, A. Najari, M. Leclerc, Synthesis of New Pyridazine-Based Monomers and Related Polymers for Photovoltaic Applications, Macromolecular Rapid Communications 31(12) (2010) 1090-1094.
[7] E.W. Culver, T.E. Anderson, J.T. López Navarrete, M.C. Ruiz Delgado, S.C. Rasmussen, Poly(thieno[3,4-b]pyrazine-alt-2,1,3-benzothiadiazole)s: A New Design Paradigm in Low Band Gap Polymers, ACS Macro Letters 7(10) (2018) 1215-1219.
[8] J. Kim, S. Chae, A. Yi, M. Kim, H.J. Kim, H. Suh, Syntheses and Properties of Semiconducting Polymers Based on Pyrimidine Series Substituted with Thiazolo-Pyridine, Macromolecular Research 26(5) (2018) 438-445.
[9] D. Gedefaw, M. Prosa, M. Bolognesi, M. Seri, M.R. Andersson, Recent Development of Quinoxaline Based Polymers/Small Molecules for Organic Photovoltaics, Advanced Energy Materials 7(21) (2017) 1700575.
[10] J. Yuan, J. Ouyang, V. Cimrová, M. Leclerc, A. Najari, Y. Zou, Development of quinoxaline based polymers for photovoltaic applications, Journal of Materials Chemistry C 5(8) (2017) 1858-1879.
[11] M. Liu, Y. Gao, Y. Zhang, Z. Liu, L. Zhao, Quinoxaline-based conjugated polymers for polymer solar cells, Polymer Chemistry 8(32) (2017) 4613-4636.
[12] S. Steinberger, A. Mishra, E. Reinold, E. Mena-Osteritz, H. Müller, C. Uhrich, M. Pfeiffer, P. Bäuerle, Synthesis and characterizations of red/near-IR absorbing A–D–A–D–A-type oligothiophenes containing thienothiadiazole and thienopyrazine central units, Journal of Materials Chemistry 22(6) (2012) 2701-2712.
[13] S.C. Rasmussen, R.L. Schwiderski, M.E. Mulholland, Thieno[3,4-b]pyrazines and their applications to low band gap organic materials, Chemical Communications 47(41) (2011) 11394-11410.
[14] L. Yang, R. Jamal, F. Liu, Y. Wang, T. Abdiryim, Structure and photocatalytic activity of a low band gap donor–acceptor–donor (D–A–D) type conjugated polymer: poly(EDOT–pyridazine–EDOT), RSC Advances 7(4) (2017) 1877-1886.

[15] S. Achelle, N. Plé, A. Turck, Incorporation of pyridazine rings in the structure of functionalized π-conjugated materials, RSC Advances 1(3) (2011) 364-388.
[16] R. Singh, A.S. Hay, Synthesis and physical properties of poly(aryl ether phthalazine)s, Macromolecules 25(3) (1992) 1025-1032.
[17] C.J. Lim, L. Li, Y. Lei, F. Zhou, B. Wu, X. Liu, F. Zhu, B.S. Ong, X. Hu, H. Su, S.-C. Ng, Synthesis and characterization of three thienopyridazine-based copolymers and their application in OFET, Tetrahedron Letters 57(14) (2016) 1523-1527.
[18] A. Albert, R. Goldacre, J. Phillips, 455. The strength of heterocyclic bases, (1948).
[19] F.P. Gabbaï, A. Schier, J. Riede, A. Schier, M.J. Hynes, Recognition of 1,2-diazines by a bidentate Lewis acid, (1998).
[20] J. Xiang, C.-L. Ho, W.-Y. Wong, Metallopolymers for energy production, storage and conservation, Polymer Chemistry 6(39) (2015) 6905-6930.
[21] W.K. Chan, Metal containing polymers with heterocyclic rigid main chains, Coordination Chemistry Reviews 251(17) (2007) 2104-2118.
[22] C.-L. Ho, W.-Y. Wong, Metal-containing polymers: Facile tuning of photophysical traits and emerging applications in organic electronics and photonics, Coordination Chemistry Reviews 255(21) (2011) 2469-2502.
[23] P.-T. Wu, T. Bull, F.S. Kim, C.K. Luscombe, S.A. Jenekhe, Organometallic Donor–Acceptor Conjugated Polymer Semiconductors: Tunable Optical, Electrochemical, Charge Transport, and Photovoltaic Properties, Macromolecules 42(3) (2009) 671-681.
[24] C. Mangeney, J.-C. Lacroix, K.I. Chane-Ching, M. Jouini, F. Villain, S. Ammar, N. Jouini, P.-C. Lacaze, Conducting-Polymer Electrochemical Switching as an Easy Means for Control of the Molecular Properties of Grafted Transition Metal Complexes, Chemistry – A European Journal 7(23) (2001) 5029-5040.
[25] L. Trouillet, A. De Nicola, S. Guillerez, Synthesis and Characterization of a New Soluble, Structurally Well-Defined Conjugated Polymer Alternating Regioregularly Alkylated Thiophene Oligomer and 2,2‘-Bipyridine Units: Metal-Free Form and Ru(II) Complex, Chemistry of Materials 12(6) (2000) 1611-1621.
[26] S.J. Higgins, Conjugated polymers incorporating pendant functional groups—synthesis and characterisation, Chemical Society Reviews 26(4) (1997) 247-257.
[27] M.L. Keshtov, S.A. Kuklin, I.O. Konstantinov, F.-C. Chen, Z.-y. Xie, G.D. Sharma, New iridium-containing conjugated polymers for polymer solar cell applications, New Journal of Chemistry 42(21) (2018) 17296-17302.
[28] W. Kin Chan, P. King Ng, X. Gong, S. Hou, Synthesis and electronic properties of conjugated polymers based on rhenium or ruthenium dipyridophenazine complexes, Journal of Materials Chemistry 9(9) (1999) 2103-2108.
[29] Y. Zhang, Z. Huang, W. Zeng, Y. Cao, Synthesis and properties of novel electrophosphorescent conjugated polyfluorenes based on aminoalkyl-fluorene and bipyridine with rhenium(I) complexes, Polymer 49(5) (2008) 1211-1219.
[30] C.W. Tse, L.S.M. Lam, K.Y.K. Man, W.T. Wong, W.K. Chan, Synthesis and characterization of random and block copolymers with pendant rhenium diimine complexes by controlled radical polymerization, Journal of Polymer Science Part A: Polymer Chemistry 43(6) (2005) 1292-1308.
[31] P.K. Ng, X. Gong, S.H. Chan, L.S.M. Lam, W.K. Chan, The Role of Ruthenium and Rhenium Diimine Complexes in Conjugated Polymers That Exhibit Interesting Opto-Electronic Properties, Chemistry – A European Journal 7(20) (2001) 4358-4367.

[32] C.S.K. Mak, W.K. Cheung, Q.Y. Leung, W.K. Chan, Conjugated Copolymers Containing Low Bandgap Rhenium(I) Complexes, Macromolecular Rapid Communications 31(9-10) (2010) 875-882.
[33] C.S.K. Mak, Q.Y. Leung, C.H. Li, W.K. Chan, Tuning the electronic properties of conjugated polymer by tethering low-bandgap rhenium(I) complex on the main chain, Journal of Polymer Science Part A: Polymer Chemistry 48(11) (2010) 2311-2319.
[34] W.K. Chan, C.S. Hui, K.Y.K. Man, K.W. Cheng, H.L. Wong, N. Zhu, A.B. Djurišić, Synthesis and photosensitizing properties of conjugated polymers that contain chlorotricarbonyl bis(phenylimino)acenaphthene rhenium(I) complexes, Coordination Chemistry Reviews 249(13) (2005) 1351-1359.
[35] M. Panigati, M. Mauro, D. Donghi, P. Mercandelli, P. Mussini, L. De Cola, G. D'Alfonso, Luminescent dinuclear rhenium(I) complexes containing bridging 1,2-diazine ligands: Photophysical properties and application, Coordination Chemistry Reviews 256(15) (2012) 1621-1643.
[36] D. Donghi, G. D'Alfonso, M. Mauro, M. Panigati, P. Mercandelli, A. Sironi, P. Mussini, L. D'Alfonso, A New Class of Luminescent Tricarbonyl Rhenium(I) Complexes Containing Bridging 1,2-Diazine Ligands: Electrochemical, Photophysical, and Computational Characterization, Inorganic Chemistry 47(10) (2008) 4243-4255.
[37] L. Veronese, E. Quartapelle Procopio, D. Maggioni, P. Mercandelli, M. Panigati, Dinuclear rhenium pyridazine complexes containing bridging chalcogenide anions: synthesis, characterization and computational study, New Journal of Chemistry 41(19) (2017) 11268-11279.
[38] A. Raimondi, M. Panigati, D. Maggioni, L. D'Alfonso, P. Mercandelli, P. Mussini, G. D'Alfonso, Electrochemical, Computational, and Photophysical Characterization of New Luminescent Dirhenium–Pyridazine Complexes Containing Bridging OR or SR Anions, Inorganic Chemistry 51(5) (2012) 2966-2975.
[39] L. Veronese, E. Quartapelle Procopio, T. Moehl, M. Panigati, K. Nonomura, A. Hagfeldt, Triarylamine-based hydrido-carboxylate rhenium(i) complexes as photosensitizers for dye-sensitized solar cells, Physical Chemistry Chemical Physics 21(14) (2019) 7534-7543.
[40] L. Veronese, E.Q. Procopio, F. De Rossi, T.M. Brown, P. Mercandelli, P. Mussini, G. D'Alfonso, M. Panigati, New dinuclear hydrido-carbonyl rhenium complexes designed as photosensitizers in dye-sensitized solar cells, New Journal of Chemistry 40(3) (2016) 2910-2919.
[41] C. Kitamura, S. Tanaka, Y. Yamashita, Design of Narrow-Bandgap Polymers. Syntheses and Properties of Monomers and Polymers Containing Aromatic-Donor and o-Quinoid-Acceptor Units, Chemistry of Materials 8(2) (1996) 570-578.
[42] A. Koutsoubelitis, K. Seintis, D. Tsikritzis, J. Oriou, C. Brochon, E. Cloutet, G. Hadziioannou, M. Vasilopoulou, S. Kennou, M. Fakis, L.C. Palilis, Photophysics, electronic structure and solar cell performance of a donor-acceptor poly(N-dodecyl-2,7-carbazole-alt-benzothiadiazole) copolymer, Organic Electronics: physics, materials, applications 59 (2018) 202-212.
[43] J. Oriou, F. Ng, G. Hadziioannou, C. Brochon, E. Cloutet, Synthesis and structure-property relationship of carbazole-alt-benzothiadiazole copolymers, Journal of Polymer Science, Part A: Polymer Chemistry 53(17) (2015) 2059-2068.
[44] J. Du, E. Xu, H. Zhong, F. Yu, C. Liu, H. Wu, D. Zeng, S. Ren, J. Sun, Y. Liu, A. Cao, Q. Fang, Alkyl side chain driven tunable red–yellow–green emission: Investigation on the new π-conjugated polymers comprising of 2,7-carbazole unit

and 2,1,3-benzo-thiadiazole units with different side chains, Journal of Polymer Science Part A: Polymer Chemistry 46(4) (2008) 1376-1387.
[45] G. Kukreja, S. Phukan, J. Kodam, D.M. More, M.V. Uravane, V.P. Palle, R.K. Kamboj, Sulfone derivatives and their use as APKM2 modulators for the treatment of cancer, PATENT WO2013005157A1, LUPIN LIMITED, 2013, p. 86.
[46] A.F. Littke, G.C. Fu, Palladium-Catalyzed Coupling Reactions of Aryl Chlorides, Angewandte Chemie International Edition 41(22) (2002) 4176-4211.
[47] C. Adamo, C. Amatore, I. Ciofini, A. Jutand, H. Lakmini, Mechanism of the Palladium-Catalyzed Homocoupling of Arylboronic Acids: Key Involvement of a Palladium Peroxo Complex, Journal of the American Chemical Society 128(21) (2006) 6829-6836.
[48] F. Lombeck, H. Komber, D. Fazzi, D. Nava, J. Kuhlmann, D. Stegerer, K. Strassel, J. Brandt, A.D. de Zerio Mendaza, C. Müller, W. Thiel, M. Caironi, R. Friend, M. Sommer, On the Effect of Prevalent Carbazole Homocoupling Defects on the Photovoltaic Performance of PCDTBT:PC71BM Solar Cells, Advanced Energy Materials 6(21) (2016) 1601232.
[49] F. Lombeck, H. Komber, S.I. Gorelsky, M. Sommer, Identifying Homocouplings as Critical Side Reactions in Direct Arylation Polycondensation, ACS Macro Letters 3(8) (2014) 819-823.
[50] S. Achelle, C. Baudequin, N. Plé, Luminescent materials incorporating pyrazine or quinoxaline moieties, Dyes and Pigments 98(3) (2013) 575-600.
[51] C. Amatore, G. Broeker, A. Jutand, F. Khalil, Identification of the Effective Palladium(0) Catalytic Species Generated in Situ from Mixtures of Pd(dba)2 and Bidentate Phosphine Ligands. Determination of Their Rates and Mechanism in Oxidative Addition, Journal of the American Chemical Society 119(22) (1997) 5176-5185.
[52] F. Samperi, S. Battiato, C. Puglisi, U. Giovanella, R. Mendichi, S. Destri, Combined techniques for the characterization of polyfluorene copolymers and correlation with their optical properties, Macromolecules 45(4) (2012) 1811-1824.
[53] E. Zhou, J. Cong, S. Yamakawa, Q. Wei, M. Nakamura, K. Tajima, C. Yang, K. Hashimoto, Synthesis of Thieno[3,4-b]pyrazine-Based and 2,1,3-Benzothiadiazole-Based Donor–Acceptor Copolymers and their Application in Photovoltaic Devices, Macromolecules 43(6) (2010) 2873-2879.
[54] S.K. Weber, F. Galbrecht, U. Scherf, Preferential Oxidative Addition in Suzuki Cross-Coupling Reactions Across One Fluorene Unit, Organic Letters 8(18) (2006) 4039-4041.
[55] S. Kappaun, M. Zelzer, K. Bartl, R. Saf, F. Stelzer, C. Slugovc, Preparation of poly(fluorene)s using trans-bis(dicyclohexylamine)palladium diacetate as a catalyst: Scope and limitations, Journal of Polymer Science Part A: Polymer Chemistry 44(6) (2006) 2130-2138.
[56] M. Jayakannan, J.L.J. van Dongen, R.A.J. Janssen, Mechanistic Aspects of the Suzuki Polycondensation of Thiophenebisboronic Derivatives and Diiodobenzenes Analyzed by MALDI–TOF Mass Spectrometry, Macromolecules 34(16) (2001) 5386-5393.
[57] L. Wen, C.L. Heth, S.C. Rasmussen, Thieno[3,4-b]pyrazine-based oligothiophenes: simple models of donor–acceptor polymeric materials, Physical Chemistry Chemical Physics 16(16) (2014) 7231-7240.
[58] C.M. Cardona, W. Li, A.E. Kaifer, D. Stockdale, G.C. Bazan, Electrochemical Considerations for Determining Absolute Frontier Orbital Energy Levels of Conjugated Polymers for Solar Cell Applications, Advanced Materials 23(20) (2011) 2367-2371.

[59] A. Zampetti, A.H. Fallahpour, M. Dianetti, L. Salamandra, F. Santoni, A. Gagliardi, M. Auf der Maur, F. Brunetti, A. Reale, T.M. Brown, A. Di Carlo, Influence of the interface material layers and semiconductor energetic disorder on the open circuit voltage in polymer solar cells, Journal of Polymer Science Part B: Polymer Physics 53(10) (2015) 690-699.
[60] T.M. Brown, F. Cacialli, Contact optimization in polymer light-emitting diodes, Journal of Polymer Science Part B: Polymer Physics 41(21) (2003) 2649-2664.
[61] G. Susanna, L. Salamandra, C. Ciceroni, F. Mura, T.M. Brown, A. Reale, M. Rossi, A. Di Carlo, F. Brunetti, 8.7% Power conversion efficiency polymer solar cell realized with non-chlorinated solvents, Solar Energy Materials and Solar Cells 134 (2015) 194-198.
[62] S. Destri, L. Veronese, S. Zappia, S. Battiato, F. Samperi, M. Panigati, Book of Abstract - New carbazole based copolymers and Rhenium-based metallo-copolymers for optoelectronic applications, Materials.it 2016 - Materials Science and Technology, Sheraton Hotel, Aci Castello, Catania, 12-16 December 2016, p. 183.
[63] J.-C. Li, E.-O. Seo, S.-H. Lee, Y.-S. Lee, Synthesis and characterization of an alternating copolymer consisting of N-(2-ethylhexyl)carbazole and 2,3-dimethylthieno[3,4-b]pyrazine units, Macromolecular Research 18(3) (2010) 304-307.
[64] H. Zhou, L. Yang, W. You, Rational Design of High Performance Conjugated Polymers for Organic Solar Cells, Macromolecules 45(2) (2012) 607-632.
[65] S. Beaupré, M. Leclerc, PCDTBT: en route for low cost plastic solar cells, Journal of Materials Chemistry A 1(37) (2013) 11097-11105.
[66] M. Mainville, M. Leclerc, Recent Progress on Indoor Organic Photovoltaics: From Molecular Design to Production Scale, ACS Energy Letters (2020) 1186-1197.

*Corresponding authors.
E-mail addresses: stefania.zappia@scitec.cnr.it (S. Zappia), f.samperi@unict.it (F. Samperi), silvia.destri@scitec.cnr.it (S. Destri)